PAPER

Check for updates

Improved efficiency and stability of flexible perovskite solar cells by a new spacer cation additive†

Xiaobo Zhang, [ID] [a] Yang Ma,[b] Xiaoqing Chen,*[b] Xuhong Li,[c] Wencai Zhou,[a] Nabonswende Aida Nadege Ouedraogo,[a] Yasuhiro Shirai, [ID] [d] Yongzhe Zhang [ID] *[b] and Hui Yan[a]

Flexible perovskite solar cells (PSCs) have attracted tremendous attention due to their potential application in portable and wearable electronics. However, the photoelectric conversion efficiency (PCE) of flexible PSCs is still far lower than that of usual rigid PSCs. Moreover, the mechanical stability of flexible PSCs cannot meet the needs of commercial applications because of the cracking of perovskite grains caused by bending stress. Here, we introduced a spacer cation additive (2-(chloromethyl) pyridine hydrochloride, CPHC) within the perovskite organic precursor to improve the device PCE and its mechanical stability. We observed that the CPHC spacer cation additive could simultaneously facilitate the crystallization of perovskite and stitch the grain boundaries to improve the flexibility. Compared to the 17.64% PCE of the control devices, the target flexible PSCs achieved a more highly efficiency over 19% with an improved mechanical stability (87.2% of the initial PCE after the 1000 cycles with the bending radius $R = 6$ mm). In addition, compared to methylammonium or formamidinium cation, due to the stronger hydrophobic and larger activation energy barrier for the ion migration of the CPHC spacer cation, the device retained over 80% of the initial PCE after 30 days storage in an ambient environment.

Introduction

To satisfy the demand for portable and wearable electronics, flexible PSCs have triggered increasing attention because of their low-cost, light weight, feasibility in roll-to-roll production.[1–4] So far, the record photoelectric conversion efficiency (PCE) of flexible PSCs is 21.1%, which is still far lower than that of rigid PSCs (25.5%).[5–7] This lower PCE can be partially attributed to the lower transmittance and the higher sheet resistance of PET/ITO substrates in comparison with conductive glasses.[8] More importantly, the issues of the perovskite crystal growth and the cracking of perovskite grains, which determines the photovoltaic performance of PSCs, are also severely restricted by a flexible substrate because the deformation of flexible substrates is usually inevitable under the annealing process.[4,9] Except for photovoltaic performance, the mechanical stability of flexible PSCs is severely affected by the fragility of ITO as well as the perovskite crystals. Therefore, high efficiency and super stability of the flexible PSCs simultaneously enhance the quality of the perovskite crystal and flexibility of the whole device.

Numerous efforts have been devoted to improve the efficiency and stability of the flexible PSCs. In terms of efficiency improvement, Yangi *et al.* reported that a novel two-dimension (2D) phenylformamidinium iodide (PFAI) cation as surface "patches" for stable flexible PSCs with the PCE of 19.89%,[8] while some other groups reported a new concept of porous planar or nanopillar arrays as an electron transport layer, achieving a PCE over 20%.[10–12] In terms of stability improvement, a bio-inspired vertebral design, a soft fullerene network and 2D perovskite as surface patches have been developed to enhance the mechanical stability of flexible PSCs.[4,8,13] Among the above methods, a 2D spacer cation as an additive has been regard as one of the most effective strategies for the simultaneous improvement of the efficiency and stability of flexible PSCs, which has been widely used in usual rigid PSCs.[14–18] Compared with 3D perovskites, 2D perovskites due to their larger organic cations than methylammonium are thermally more robust. These lager cations can hamper internal ionic motion as well as endow the perovskite layer with the much needed hydrophobic character through adequate organic moieties leading to an improved stability.[19,20] Based on a previous report,[20] a novel type larger organic spacer cation is chosen, which is expected to be better than the most intensely studied 3D perovskite cations.[19,20]

[a]*College of Material Sciences and Engineering, Beijing University of Technology, Beijing 100124, China*

[b]*Key Laboratory of Optoelectronics Technology, Ministry of Education, Faculty of Information Technology, Beijing University of Technology, Beijing 100124, China. E-mail: chenxiaoqing@bjut.edu.cn; yzzhang@bjut.edu.cn*

[c]*School of Physics, Beihang University, Beijing 100191, China*

[d]*National Institute for Materials Science (NIMS), 1-1 Namiki, Tsukuba, Ibaraki, 305-0044, Japan*

† Electronic supplementary information (ESI) available. See DOI: 10.1039/d1ra05399j

Herein, we propose the use of a novel 2D perovskite material based on a large size 2-(chloromethyl) pyridine hydrochloride (CPHC) as the spacer cation additive to fabricate highly efficient and super stable flexible PSCs, which benefits from the pyridine group and chloride anion in CPHC. The chloride ion is a widely used additive used to improve the crystallinity of perovskite films, which consequently reduce defect state density,[21,22] while pyridine groups have a similar effect.[23–25] For example, when a pyridine group is incorporated into a perovskite film, it has strong interaction with Pb^{2+} ions, which control perovskite crystallization to suppress the morphological defect formation, resulting in a high-quality perovskite film with larger grains and lower defects.[24] In addition, when the pyridine group acts as an interfacial modifier between the hole transport layer and perovskite, it can enhance hole extraction, increase hole mobility and conductivity of the hole transport layer, reduce defect density, and retard interfacial charge recombination.[23,25] Based on the above-mentioned reasons, we chose CPHC as the additive to improve the PSC performance.

By the optimization of the concentration of the CPHC spacer cation additive, we obtained a photomask aperture area of 0.04 cm^2 flexible PSCs, with a high efficiency over 19% for reverse scan (RS). Moreover, the CPHC spacer cation additive could simultaneously facilitate the crystallization of perovskite on a flexible substrate as well as stitch the grain boundary to improve the flexibility. The resultant flexible PSCs achieved a steady-state efficiency of 18.71% with a strong mechanical stability, which retained the 87.2% of the initial PCE after the 1000 cycles with the bending radius $R = 6$ mm. In addition, due to the hydrophobic and larger activation energy barrier for the ion migration of the CPHC spacer cation compared with MA or FA cation,[26–33] the target device retained over 80% of the initial efficiency after 30 days of storage in an ambient environment.

Results and discussion

The structure of the flexible PSCs is illustrated in Fig. 1a, consisting of PET/ITO/SnO_2/$FA_xMA_{1-x}PbI_yCl_{1-y}$/spiro-OMeTAD/Au, respectively. The FA-based mixed perovskite film is fabricated according to a previously reported procedure.[9,34] The experiment details are given in the ESI.† The flexible PSCs possess the advantages of being light-weight, low-cost, and flexibile, which make them suitable for use in wearable electronics, intelligent vehicles, and building-integrated photovoltaics.[1,4] However, stretching or bending can destroy the perovskite film, leading to the formation of cracks at the grain boundaries and the deformation of the crystal structure (Fig. 1c).[9] To address this problem, a new type organic spacer CPHC acts as an adhesive between perovskite grains to improve the mechanical stability of flexible PSCs,[8] as shown in Fig. 1b. Moreover, the incorporated CPHC can form an 2D/3D perovskite network, as shown in Fig. 1d. The 2D/3D perovskite network effectively absorbs and releases the stress, and the target film is expected to exhibit better mechanical stability under stretching or bending.[13]

To investigate the effect of the organic spacer CPHC on the photovoltaic performance, the current density and voltage (J–V) characteristics under AM 1.5G illumination with the light
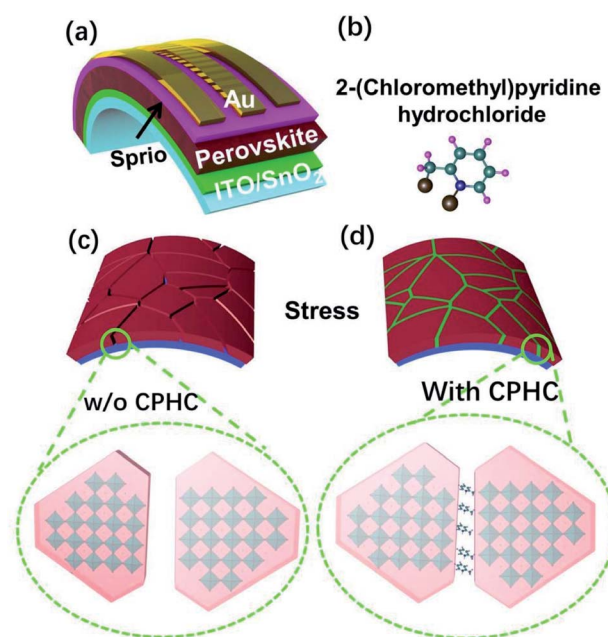

Fig. 1 (a) Architecture of a flexible perovskite solar cell. (b) The molecular structure of 2-(chloromethyl) pyridine hydrochloride. Schematic of the perovskite's grain boundary without (c) and with (d) the CPHC treatment.

intensity of 100 mW cm^{-2} were carried out. The J–V curves and the corresponding photovoltaic parameters are shown in Fig. 2a and the inset of the same figure, respectively. The control device shows the champion PCE of 17.64%, with an open circuit voltage (V_{OC}) of 1.07 V, short-circuit current density (J_{SC}) of 22.28 mA cm^{-2}, and fill factor (FF) of 0.74. The target device delivers an increased PCE of 19.32%, with V_{OC} of 1.10 V, J_{SC} of 22.52 mA cm^{-2}, and FF of 0.78. According to the characterization results mentioned above, it has been proved that the incorporated CPHC spacer cation additive can improve the V_{OC} and FF significantly, while the J_{SC} remained almost similar. As shown in Fig. 2b, the mismatch between the integral current obtained from EQE (21.89 mA cm^{-2} of the target device) and the short-circuit current of the J–V curve is less than 5%, indicating the feasibility of our J–V curve results. As shown in Fig. 2c, 20 target devices were statistically evaluated, showing an average PCE of 18.13%, which is superior to the control devices having a PCE of 16.47% (other photovoltaic statistics as Fig. S1†). It is statistically verified that the addition of CPHC leads to a higher PCE. Steady-state photocurrent and efficiency have been measured at the maximum power point of 0.92 V for over 300 s to investigate the light-soaking stability (Fig. 2d). The efficiency of the target devices is stabilized at 18.71%, showing an excellent light-soaking stability during the measurement.

In addition, the J–V hysteresis behavior of the target device is observed to have an obvious decline (as Fig. 2e and f), compared with that of the control device, resulting from the incorporated CPHC spacer cation additive suppression ion migration.[35,36] Based on previous reports,[32,36,37] the 2D/3D perovskite network in Fig. 1d is more persuasive in explaining the smaller
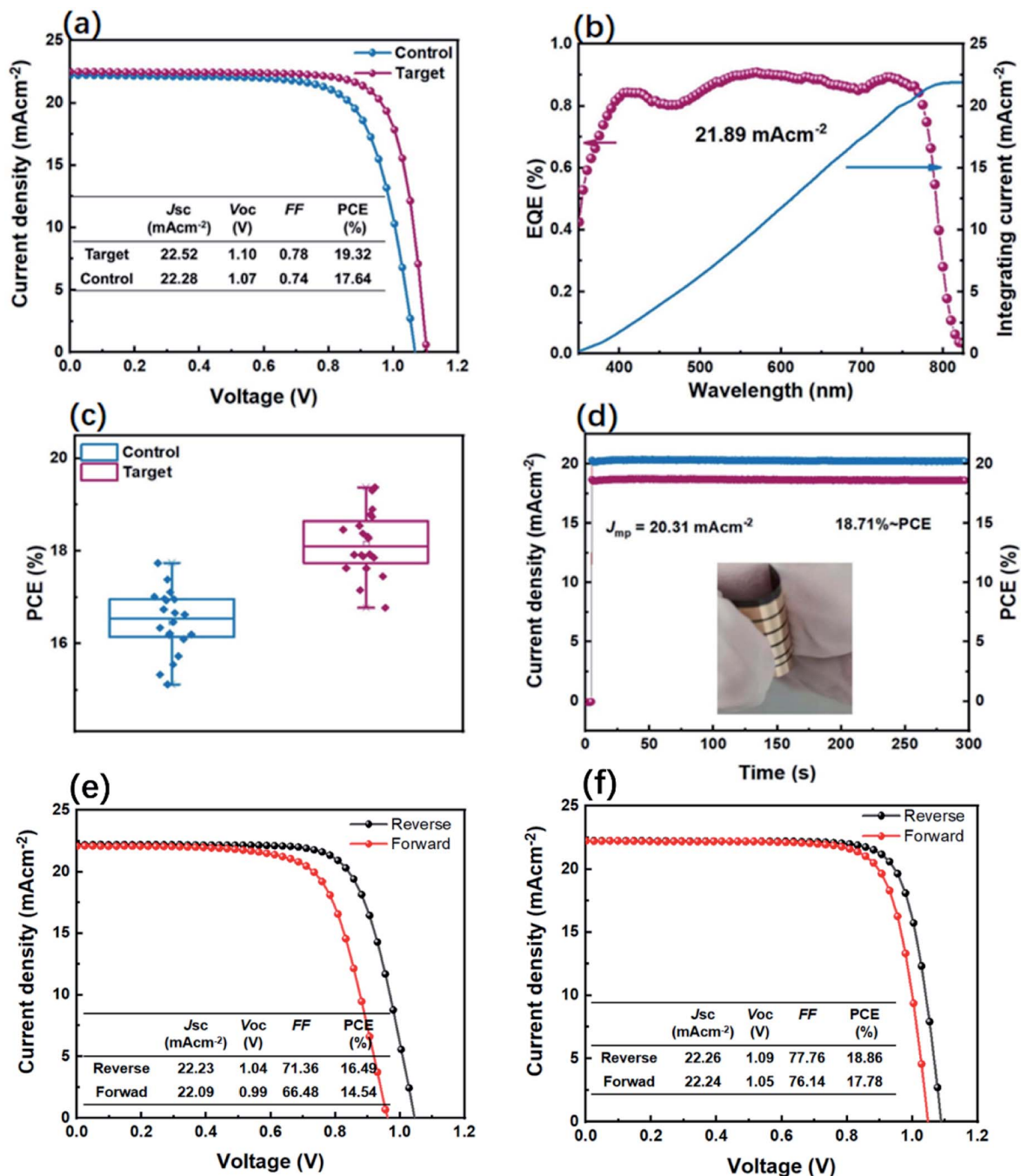
Fig. 2 (a) The champion J–V curves of the control and target device. (b) The corresponding EQE spectra of the target device. (c) The PCE statistics of the control and target devices. (d) Steady-state photocurrent and efficiency of the target device. The J–V curves of the control (e) and target (f) device for reverse scan and forward scan.

hysteresis behavior of the incorporated CPHC into the perovskite because 2D perovskites mixed in 3D perovskites grain cannot effectively suppress the hysteresis behavior caused by ion migration. As intensely discussed,[35,38] there are three possible origins, which could be responsible for the hysteresis, namely (1) bulk or surface defects of perovskite, which act as traps for charges, (2) ferroelectric polarization of the perovskite and (3) excess mobile ions. Among these reasons, the cause of hysteresis induced by defects and defect ions migration has

been proved by theoretical and experimental investigation.[39–41] These defects are most easily formed at grain boundaries and surfaces.[42] In this article, we consider that the CPHC additive could reduce the trap density. Nevertheless, there are still residual defects in the interface between the perovskite and hole/electron transport layer as confirmed by the DLCP results (Fig. 4d). In this regard, the hysteresis phenomenon is still present in our passivated device, suggesting further interface passivation is required.
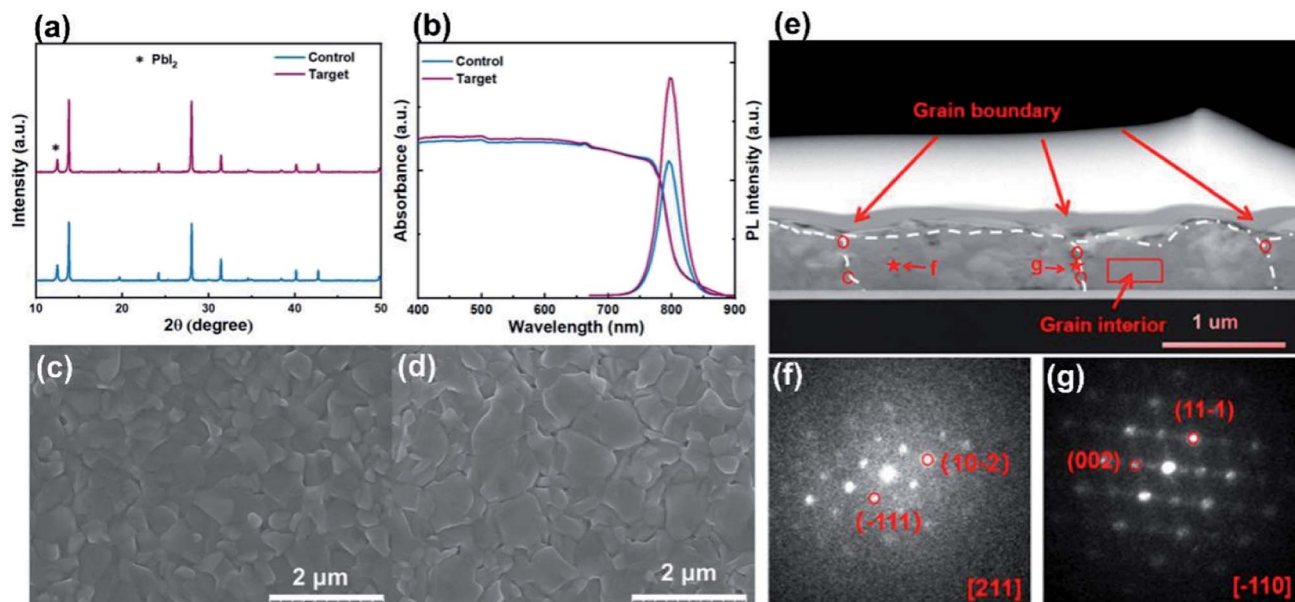
Fig. 3 (a) XRD patterns, (b) UV-vis spectra and steady-state PL images, SEM image of the control (c) and target (d) perovskite films. (e) The cross-section HAADF-STEM images of the target perovskite film. EDS was carried out on the grain interior (red rectangle) and grain boundary (red circle). The nano-beam electron diffraction patterns on the grain interior (f) and grain boundary (g).

Fig. 3a shows the XRD patterns of the control and target perovskite films. The main diffraction peaks for target film at 14.3° and 28.5°, corresponding to (110) and (220) lattice planes of the 3D perovskite film, respectively, cannot find an obvious peak location shift in comparison with these for the control film, implying that the additive cannot change the original phase structure.[34] In addition, the PbI_2 peaks at 12.5° indicate the incomplete conversion from PbI_2 to $FAPbI_3$, and the moderate residual of PbI_2 can improve the performance of PSCs.[43–45] Moreover, we employed the peak-to-peak intensity ratio to show the XRD peak intensity change caused by the incorporation of CPHC spacers. As shown in Fig. 3a, the strongest peaks of PbI_2 and perovskite are located at 12.5° and 13.7°, respectively. As the following Fig. S2,† we have calculated the corresponding XRD peak intensity ratio, which is positively correlated with the content of PbI_2 and perovskite in the film.[46] Therefore, the strongest XRD peak intensity ratio of the perovskite to PbI_2 can be used to illustrate the crystalline behavior of the perovskite. After the incorporation of CPHC spacers, the peak intensity ratio of the perovskite to PbI_2 increases from 3.75 to 5.90, indicating that CPHC can promote the crystallization of the perovskite and inhibit the formation of PbI_2.[34,43,47,48] Fig. 3b shows the ultraviolet-visible (UV-vis) absorption spectra and steady-state photoluminescence (PL) of control and target perovskite films. Compared with the control film, the target perovskite films exhibit nearly similar onset absorption and PL peaks, indicating an unchanged optical bandgap. However, under the same excitation and detection condition, the target perovskite has slightly higher absorbance (400–750 nm) and stronger PL intensity than the control perovskite, demonstrating the higher quality of the target perovskite film.[1] This is further supported by the next scanning electron microscopy

(SEM) results. The top-view SEM images (Fig. 3c and d) reflect that the organic spacer CPHC promotes the crystallization of perovskite films and significantly increases the overall grain size. The average grain size for target perovskite films is about 0.45 μm, which is much larger than 0.31 μm for the control perovskite films (the corresponding particle size statistics shown in Fig. S3†). The enlarged grain size can bring a positive impact on the device performance, confirmed by the $J–V$ results.[49]

In order to prove that the additive molecules are at the grain boundary, we carried out relevant experiments, including Fourier transform infrared spectroscopy (FTIR), high-angle annular dark-field scanning transmission electron microscopy (HAADF-STEM), energy disperse spectroscopy (EDS) and nano-beam electron diffraction (NBD). In the FTIR results (Fig. S4†), after incorporating the CPHC, three peaks belonging to the piperidyl group from CPHC (around 1420, 1485 and 1527 cm^{-1}) can be observed. In addition, the peak corresponding to the perovskite shifts from 1470 cm^{-1} to 1475 cm^{-1}. These results indicate that the additive can interact with the component of the perovskite and control its growth.[24] Fig. 3g displays the cross-section HAADF-STEM of the perovskite film with the additive CPHC treatment, and the cross section of the perovskite consists of four grains (three grain boundaries). On the basis of the high-resolution cross-section HAADF-STEM images, we further carried out EDS on the grain interior (red rectangle) and grain boundary (red circle). We found that the average I : Pb ratio is 2.84 in the interior of the grain, while the ratio is 2.92 at the grain boundary. The general chemical formula of the perovskite film without and with the additive CPHC is ABX_3 and $A'A_{n-2}B_nX_{3n+1}$, respectively, where A, A′, B and X represent FA^+, $CPHC^{2+}$, Pb^{2+} and halide ions, respectively.

Based on the difference of the above general chemical formula, we can infer that the I : Pb ratio of the perovskite film increases after the incorporation of CPHC. Therefore, the average I : Pb ratio at the grain boundary is higher than that in the interior of the grain, which can support that the additive CPHC mainly exists at grain boundaries. To further confirm that the additive is at the grain boundary, NBD has been carried out to investigate the crystal structure evolution for two individual areas (red star), as shown in Fig. 3g and h. The zone axis of grain internal areas is obviously different from that of grain boundary areas, suggesting a polycrystalline perovskite layer. After careful calibration of all measured diffraction patterns, we found that the crystal plane distance at the grain boundary increased with respect to that in the interior of the grain. The crystal plane distance of (-111) and $(11-1)$ planes were measured to be 3.46 and 3.75 Å for two individual areas, respectively, which is consistent with that of the perovskite as the incorporation of CPHC causes lattice constant expansion.

We have further confirmed the effects of the CPHC incorporation on the electron dynamics of the control and target PSCs by transient photovoltage (TPV). As shown in the TPV results (Fig. 4a), the control device shows a faster decay than the target device, indicating more effective charge extraction and longer carrier lifetime in the target device.[10] This increased charge extraction, which can be ascribed to more effective electron transfer from the perovskite to the carrier transport layer as well as improved crystallinity and enlarged grain size of the perovskite layer by the incorporated CPHC organic spacer. Increased lifetime comes from the reduced trap density in the perovskite layer, as confirmed by the next measurements (such as space-charge limited current). In order to confirm the suppression of electric traps by the CPHC spacer cation additive, we fabricated an electron-only device with the configuration of the PET/ITO/SnO$_2$/perovskite (with or without the incorporated CPHC spacer cation additive)/PCBM/Au. The double logarithmic J–V plots (Fig. 4b) were measured under dark conditions. According to the space-charge limited current (SCLC) theory,[45] we know the corresponding electric trap densities for the target and control device are 1.49×10^{15} and 2.08×10^{15} cm^{-3}, respectively. In addition, the relationship between V_{OC} and light intensity is (Fig. 4c) analyzed for the ideality factor (n) of the control device (1.449) and that of the target device (1.182), using the equation: $V_{OC} = \frac{nK_BT}{q}\ln(J_{SC}/J_0 + 1)$, where J_0 is the dark saturation current density, q is the elementary charge, K_B is the Boltzmann constant and T is the temperature, respectively.[11,42] The lowered ideality factor of the target device indicates suppressed trap-
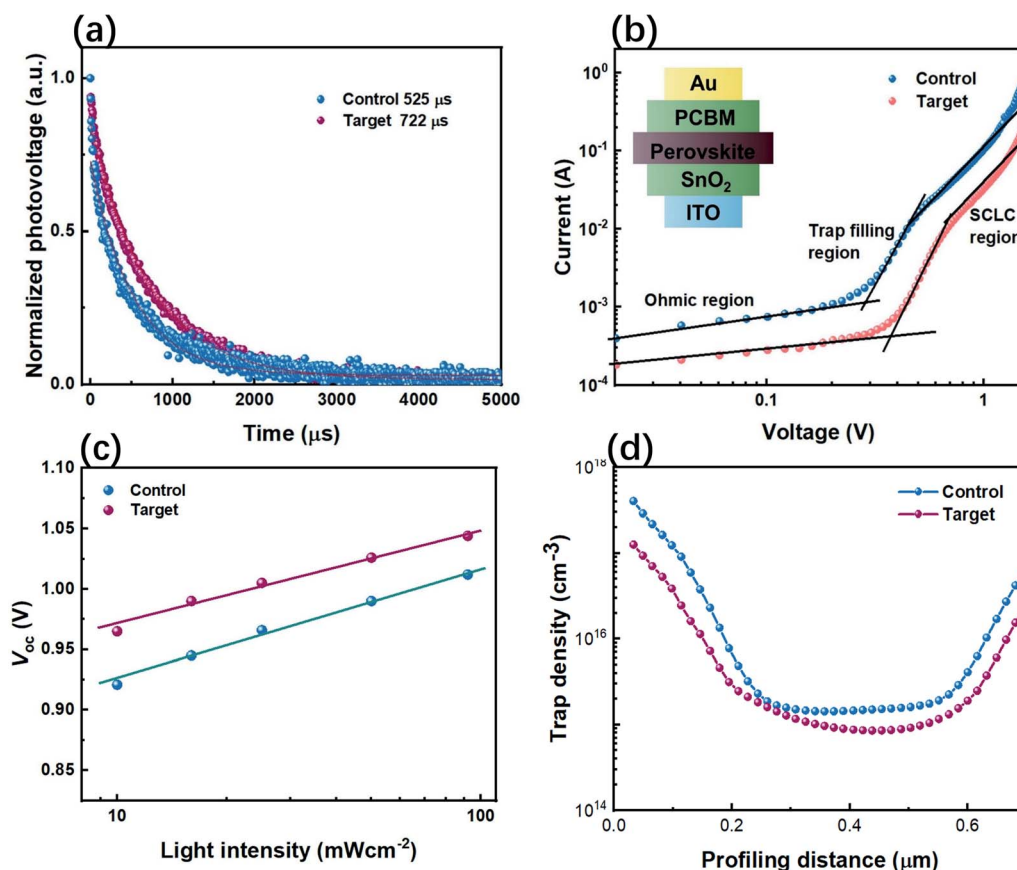

Fig. 4 (a) Transient photovoltage curves of the different flexible PSCs. (b) Dark J–V curves of the electron-only devices with the different perovskite films. The inset shows the configuration of the devices. (c) Relationship between V_{OC} and light intensity for different devices. (d) The distribution of defects in the perovskite layer obtained by DLCP at 10 kHz with and without the CPHC treatment.

assisted recombination (SRH recombination) in this device.[42] The suppression of traps results in the enhanced built-in potential, as confirmed by capacitance–voltage curves (Fig. S5†). Furthermore, the drive-level capacitance profiling (DLCP) method based on an alternate capacitance technique has been performed to provide the spatial distribution of trap density in the band gap of the control and target perovskite film.[50] The DLCP measurements have been performed at ac frequency of 10 kHz by subtracting the free carrier density measured at high ac frequencies (500 kHz) from the total carrier density measured at the 10 kHz frequency. A symmetric spatial distribution of the trap density is shown in Fig. 4d. Compared with that of the control device, minimal bulk trap density of the target device shows a significant reduction from 1.43×10^{15} to 8.52×10^{14} cm^{-3}. This result indicates that the CPHC additive can passivate the defect inside the bulk, more possibly passivating the defect at the grain boundary,[51] which is consistent with the above SCLC results. The grain boundary is the place where defects are most easily formed, where the crystal structure is suddenly interrupted, leading to product dangling bonds.[37,42,51] Therefore, according to the above-mentioned results about defect characterization, it can be reasonably speculated that the CPHC additive mainly passivates the defects at the grain boundary (as shown in Fig. 1d).

In order to evaluate the mechanical stability of flexible PSCs, the efficiency variations for different PSCs were monitored throughout 200 consecutive bending cycles. The finally conserved PCE of different bending radii ($R = 12, 9, 6,$ and 3 mm, respectively) are shown in Fig. 5a. After 200 cycles with 12 mm, 9 mm, 6 mm or 3 mm bending radius, the PCE of PSCs based on the target device can still maintain about 99.2%, 97.9%, 97.1% and 93.9% of the initial PCE, respectively. However, the PCE for the control devices decreases significantly, only 98.4%, 96.1%, 91.8% and 81.1% of the original PCE can be retained, which directly proves that the incorporated CPHC spacer can improve the mechanical stability and bending-endurance of flexible PSCs. Moreover, when the bending angle continues to increase, a noticeable decrease in the control device's PCE begins to appear at the bending radius of $R = 6$ mm, implying that the bending radius limit of ITO is 6 mm.[4] Therefore, the relationship between PCE and bending cycles with the bending radius of $R = 6$ mm has been measured (Fig. 5b). After increasing the cycles to 1000, the target and control device can maintain 87.2% and 70.7% of the initial PCE, respectively. These results have proved that the incorporation CPHC spacer into the perovskite can efficiently improve the mechanical stability, subsequently providing extreme universality for wearable applications. The long-term environment stability of the PSCs with or without the CPHC treatment was studied by exposing them to an ambient and dark environment for 30 days (relative humidity of 30–60%). We notice that the PCE of the target PSCs exhibits an excellent stability with
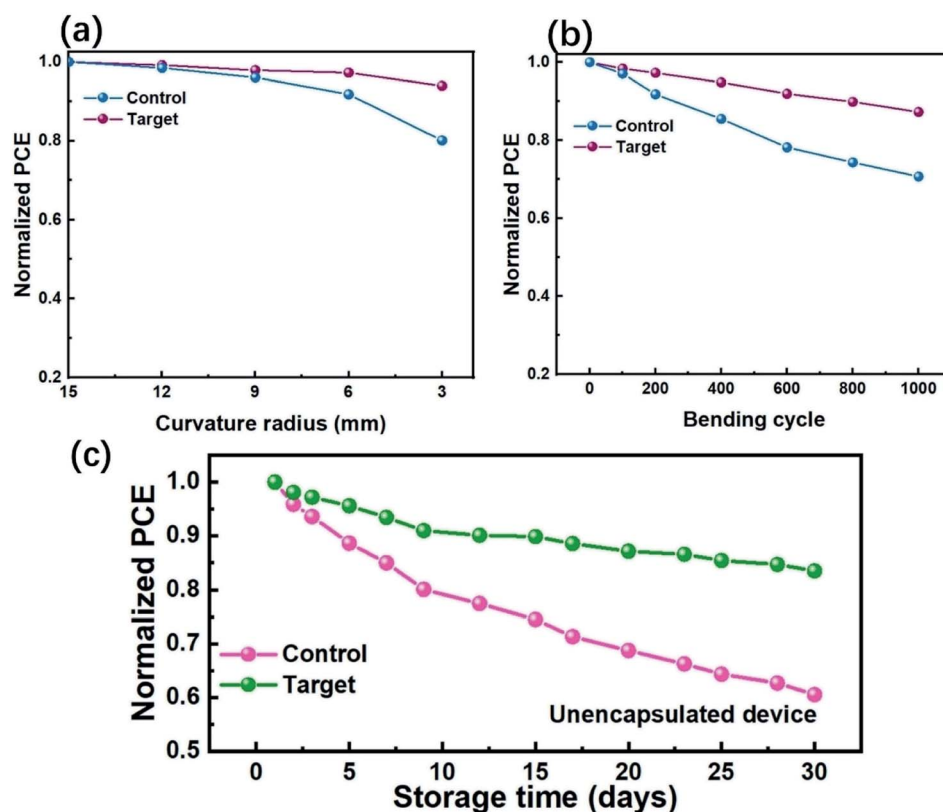

Fig. 5 (a) Normalized PCE value for the flexible PSCs after bending 200 cycles with different bending radii. (b) Normalized PCE value for the flexible PSCs as a function of bending cycles with a radius of 6 mm. (c) Stability characteristics of the different flexible PSCs performed under ambient air conditions.

a much slower degradation rate and retains 83.5% of its initial value, compared to the PCE of the control device, which has shown a fast decrease at 60.5% of its initial value after storage of 30 days (Fig. 5c). The enhanced stability of the target devices is mainly attributed to the efficient defect passivation as well as the robust moisture resistant at the perovskite grain boundaries with the assistance of the CPHC spacer incorporation because the defects at the perovskite surface and grain boundaries are one of the main reasons for the accelerated moisture infiltration into the perovskite layer.[52,53]

Conclusion

In summary, we introduced a new spacer cation additive (CPHC) within the perovskite organic precursor to the efficiency and stability of the flexible PSCs. The significant effect of CPHC in perovskite films was proven to stitch the perovskite grains *via* facilitating the crystallization of perovskite. Benefiting from the CPHC spacer cation additive incorporation, the excellent flexible PSCs exhibit PCE values of 19.32% as measured from the reverse scan due to the suppression of the traps at grain boundary. In addition, the target flexible devices display a strong mechanical stability and environment stability, which maintained 87.2% of the initial PCE after the 1000 cycles with the bending radius $R = 6$ mm, and retained over 80% of the initial PCE after 30 days storage in an ambient environment. This study presents a significant insight for improving perovskite film qualities by using 2-(chloromethyl) pyridine hydrochloride for further achieving high-performance flexible PSCs and optoelectronic devices.

Conflicts of interest

There are no conflicts to declare.

Acknowledgements

References

1 T. Bu, J. Li, F. Zheng, W. Chen, X. Wen, Z. Ku, Y. Peng, J. Zhong, Y. B. Cheng and F. Huang, Universal passivation strategy to slot-die printed SnO2 for hysteresis-free efficient flexible perovskite solar module, *Nat. Commun.*, 2018, **9**, 4609.

2 D. Yang, R. Yang, S. Priya and S. Liu, Recent Advanced in Flexible Perovskite Solar Cell: Fabrication and Application, *Angew. Chem., Int. Ed.*, 2019, **58**, 4466–4483.

3 C. Jia, X. Zhao, Y.-H. Lai, J. Zhao, P.-C. Wang, D.-S. Liou, P. Wang, Z. Liu, W. Zhang, W. Chen, Y.-H. Chu and J. Li, Highly flexible, robust, stable and high efficiency perovskite solar cells enabled by van der Waals epitaxy on mica substrate, *Nano Energy*, 2019, **60**, 476–484.

4 X. Meng, Z. Cai, Y. Zhang, X. Hu, Z. Xing, Z. Huang, Z. Huang, Y. Cui, T. Hu, M. Su, X. Liao, L. Zhang, F. Wang, Y. Song and Y. Chen, Bio-inspired vertebral design for scalable and flexible perovskite solar cells, *Nat. Commun.*, 2020, **11**, 3016.

5 L. Yang, Q. Xiong, Y. Li, P. Gao, B. Xu, H. Lin, X. Li and T. Miyasaka, Artemisinin-passivated mixed-cation perovskite films for durable flexible perovskite solar cells with over 21% efficiency, *J. Mater. Chem. A*, 2021, **9**, 1574–1582.

6 B.-W. Park, H. W. Kwon, Y. Lee, D. Y. Lee, M. G. Kim, G. Kim, K.-J. Kim, Y. K. Kim, J. Im, T. J. Shin and S. I. Seok, Stabilization of formamidinium lead triiodide α-phase with isopropylammonium chloride for perovskite solar cells, *Nat. Energy*, 2021, **6**, 419–428.

7 National Renewable Energy Laboratory, *Best research-cell efficiencies chart*, https://www.nrel.gov/pv/cell-efficiency.html.

8 L. Yangi, Y. Li, Y. Pei, J. Wang, H. Lin and X. Li, A novel 2D perovskite as surface "patches" for efficient flexible perovskite solar cells, *J. Mater. Chem. A*, 2020, **8**, 7808–7818.

9 Y. Y. Xiao, Y. Meng, H. Gao, Y. Chen, Q. Meng, Y. Bai, H. Wang, Y. Zhang, H. Yan and C. B. Han, Flexible perovskite solar cells fabricated by a gradient heat treatment process, *Sustainable Energy Fuels*, 2020, **4**, 824–831.

10 J. Chung, S. S. Shin, K. Hwang, G. Kim, K. W. Kim, D. S. Lee, W. Kim, B. S. Ma, Y.-K. Kim, T.-S. Kim and J. Seo, Record-efficiency flexible perovskite solar cell and module enabled by a porous-planar structure as an electron transport layer, *Energy Environ. Sci.*, 2020, **13**, 4854–4861.

11 S. Cong, G. Zou, Y. Lou, H. Yang, Y. Su, J. Zhao, C. Zhang, P. Ma, Z. Lu, H. Fan and Z. Huang, Fabrication of Nickel Oxide Nanopillar Arrays on Flexible Electrodes for Highly Efficient Perovskite Solar Cells, *Nano Lett.*, 2019, **19**, 3676–3683.

12 J. Sun, Q. Hua, R. Zhou, D. Li, W. Guo, X. Li, G. Hu, C. Shan, Q. Meng, L. Dong, C. Pan and Z. L. Wang, Piezo-Phototronic Effect Enhanced Efficient Flexible Perovskite Solar Cells, *ACS Nano*, 2019, **13**, 4507–4513.

13 M. Li, Y. G. Yang, Z. K. Wang, T. Kang, Q. Wang, S. H. Turren-Cruz, X. Y. Gao, C. S. Hsu, L. S. Liao and A. Abate, Perovskite Grains Embraced in a Soft Fullerene Network Make Highly Efficient Flexible Solar Cells with Superior Mechanical Stability, *Adv. Mater.*, 2019, **31**, 1901519.

14 J. Chen, J.-Y. Seo and N.-G. Park, Simultaneous Improvement of Photovoltaic Performance and Stability by In Situ Formation of 2D Perovskite at $(FAPbI_3)_{0.88}(CsPbBr_3)_{0.12}$/CuSCN Interface, *Adv. Energy Mater.*, 2018, **8**, 1702714.

15 G. Grancini, C. Roldán-Carmona, I. Zimmermann, E. Mosconi, X. Lee, D. Martineau, S. Narbey, F. Oswald, F. De Angelis, M. Graetzel and M. K. Nazeeruddin, One-Year stable perovskite solar cells by 2D/3D interface engineering, *Nat. Commun.*, 2017, **8**, 15684.

16 T. M. Koh, V. Shanmugam, X. Guo, S. S. Lim, O. Filonik, E. M. Herzig, P. Müller-Buschbaum, V. Swamy, S. T. Chien,

S. G. Mhaisalkar and N. Mathews, Enhancing moisture tolerance in efficient hybrid 3D/2D perovskite photovoltaics, *J. Mater. Chem. A*, 2018, **6**, 2122–2128.

17 D. Lin, T. Zhang, J. Wang, M. Long, F. Xie, J. Chen, B. Wu, T. Shi, K. Yan, W. Xie, P. Liu and J. Xu, Stable and scalable 3D-2D planar heterojunction perovskite solar cells via vapor deposition, *Nano Energy*, 2019, **59**, 619–625.

18 Y. Lin, Y. Bai, Y. Fang, Z. Chen, S. Yang, X. Zheng, S. Tang, Y. Liu, J. Zhao and J. Huang, Enhanced Thermal Stability in Perovskite Solar Cells by Assembling 2D/3D Stacking Structures, *J. Phys. Chem. Lett.*, 2018, **9**, 654–658.

19 A. Krishna, S. Gottis, M. K. Nazeeruddin and F. Sauvage, Mixed Dimensional 2D/3D Hybrid Perovskite Absorbers: The Future of Perovskite Solar Cells?, *Adv. Funct. Mater.*, 2018, **29**, 1806482.

20 L. Mao, C. C. Stoumpos and M. G. Kanatzidis, Two-Dimensional Hybrid Halide Perovskites: Principles and Promises, *J. Am. Chem. Soc.*, 2018, **141**, 1171–1190.

21 J. Chen, X. Zhao, S. G. Kim and N. G. Park, Multifunctional Chemical Linker Imidazoleacetic Acid Hydrochloride for 21% Efficient and Stable Planar Perovskite Solar Cells, *Adv. Mater.*, 2019, **31**, 1902902.

22 H. Jiang, Z. Yan, H. Zhao, S. Yuan, Z. Yang, J. Li, B. Liu, T. Niu, J. Feng, Q. Wang, D. Wang, H. Yang, Z. Liu and S. F. Liu, Bifunctional Hydroxylamine Hydrochloride Incorporated Perovskite Films for Efficient and Stable Planar Perovskite Solar Cells, *ACS Appl. Energy Mater.*, 2018, **1**, 900–909.

23 H. Cheng, Y. Li, G. Zhao, K. Zhao and Z. S. Wang, Pyridine-Terminated Conjugated Organic Molecules as an Interfacial Hole Transfer Bridge for NiOx-Based Perovskite Solar Cells, *ACS Appl. Mater. Interfaces*, 2019, **11**, 28960–28967.

24 S. Fu, X. Li, L. Wan, Y. Wu, W. Zhang, Y. Wang, Q. Bao and J. Fang, Efficient Passivation with Lead Pyridine-2-Carboxylic for High-Performance and Stable Perovskite Solar Cells, *Adv. Energy Mater.*, 2019, **9**, 1901852.

25 X. Zhao, J. Zhou, S. Wang, L. Tan, M. Li, H. Li and C. Yi, Effects of N-Positions on Pyridine Carboxylic Acid-Modified Inverted Perovskite Solar Cells, *ACS Appl. Energy Mater.*, 2021, **4**, 6903–6911.

26 C. Chen, Z. Song, C. Xiao, R. A. Awni, C. Yao, N. Shrestha, C. Li, S. S. Bista, Y. Zhang, L. Chen, R. J. Ellingson, C.-S. Jiang, M. Al-Jassim, G. Fang and Y. Yan, Arylammonium-Assisted Reduction of the Open-Circuit Voltage Deficit in Wide-Bandgap Perovskite Solar Cells: The Role of Suppressed Ion Migration, *ACS Energy Lett.*, 2020, **5**, 2560–2568.

27 Z. Huang, A. H. Proppe, H. Tan, M. I. Saidaminov, F. Tan, A. Mei, C.-S. Tan, M. Wei, Y. Hou, H. Han, S. O. Kelley and E. H. Sargent, Suppressed Ion Migration in Reduced-Dimensional Perovskites Improves Operating Stability, *ACS Energy Lett.*, 2019, **4**, 1521–1527.

28 Y. Lin, Y. Bai, Y. Fang, Q. Wang, Y. Deng and J. Huang, Suppressed ion migration in Low-dimensional perovskites, *ACS Energy Lett.*, 2017, **2**, 1571–1572.

29 W. Peng, C. Aranda, O. M. Bakr, G. Garcia-Belmonte, J. Bisquert and A. Guerrero, Quantification of Ionic Diffusion in Lead Halide Perovskite Single Crystals, *ACS Energy Lett.*, 2018, **3**, 1477–1481.

30 D. Sirbu, F. H. Balogun, R. L. Milot and P. Docampo, Layered Perovskites in Solar Cells: Structure, Optoelectronic Properties, and Device Design, *Adv. Energy Mater.*, 2021, **11**, 2003877.

31 T. Zhang, C. Hu and S. Yang, Ion Migration: A "Double-Edged Sword" for Halide-Perovskite-Based Electronic Devices, *Small Methods*, 2019, **4**, 1900552.

32 Y. Shao, Y. Fang, T. Li, Q. Wang, Q. Dong, Y. Deng, Y. Yuan, H. Wei, M. Wang, A. Gruverman, J. Shield and J. Huang, Grain boundary dominated ion migration in polycrystalline organic–inorganic halide perovskite films, *Energy Environ. Sci.*, 2016, **9**, 1752–1759.

33 X. Jiang, J. Zhang, S. Ahmad, D. Tu, X. Liu, G. Jia, X. Guo and C. Li, Dion-Jacobson 2D-3D perovskite solar cells with improved efficiency and stability, *Nano Energy*, 2020, **75**, 104892.

34 T. Liu, J. Guo, D. Lu, Z. Xu, Q. Fu, N. Zheng, Z. Xie, X. Wan, X. Zhang, Y. Liu and Y. Chen, Spacer Engineering Using Aromatic Formamidinium in 2D/3D Hybrid Perovskites for Highly Efficient Solar Cells, *ACS Nano*, 2021, **15**, 7811–7820.

35 D. H. Kang and N. G. Park, On the Current-Voltage Hysteresis in Perovskite Solar Cells: Dependence on Perovskite Composition and Methods to Remove Hysteresis, *Adv. Mater.*, 2019, **31**, e1805214.

36 J. Chen, D. Lee and N. G. Park, Stabilizing the Ag Electrode and Reducing J-V Hysteresis through Suppression of Iodide Migration in Perovskite Solar Cells, *ACS Appl. Mater. Interfaces*, 2017, **9**, 36338–36349.

37 L. Liu, S. Huang, Y. Lu, P. Liu, Y. Zhao, C. Shi, S. Zhang, J. Wu, H. Zhong, M. Sui, H. Zhou, H. Jin, Y. Li and Q. Chen, Grain-Boundary "Patches" by In Situ Conversion to Enhance Perovskite Solar Cells Stability, *Adv. Mater.*, 2018, **30**, 1800544.

38 M. Y. Bo Chen, S. Priya and K. Zhu, Origin of J−V Hysteresis in Perovskite Solar Cells, *J. Phys. Chem. Lett.*, 2016, **7**, 905–917.

39 G. Richardson, S. E. J. O'kane, R. G. Niemann, T. A. Peltola, J. M. Foster, P. J. Cameron and A. B. Walker, Can slow-moving ions explain hysteresis in the current–voltage curves of perovskite solar cells?, *Energy Environ. Sci.*, 2016, **9**, 1476–1485.

40 G. Xia, B. Huang, Y. Zhang, X. Zhao, C. Wang, C. Jia, J. Zhao, W. Chen and J. Li, Nanoscale insights into photovoltaic hysteresis in triple-cation mixed-halide perovskite: resolving the role of polarization and ionic migration, *Adv. Mater.*, 2019, **31**, 1902870.

41 Y. Zhang, M. Liu, G. E. Eperon, T. C. Leijtens, D. Mcmeekin, M. Saliba, W. Zhang, M. De Bastiani, A. Petrozza, L. M. Herz, M. B. Johnston, H. Lin and H. J. Snaith, Charge selective contacts, mobile ions and anomalous hysteresis in organic–inorganic perovskite solar cells, *Mater. Horiz.*, 2015, **2**, 315–322.

42 Q. Jiang, Y. Zhao, X. Zhang, X. Yang, Y. Chen, Z. Chu, Q. Ye, X. Li, Z. Yin and J. You, Surface passivation of perovskite film for efficient solar cells, *Nat. Photonics*, 2019, **13**, 460–466.

43 K. Li, J. Xiao, X. Yu, T. Li, D. Xiao, J. He, P. Zhou, Y. Zhang, W. Li, Z. Ku, J. Zhong, F. Huang, Y. Peng and Y. Cheng, An efficient, flexible perovskite solar module exceeding 8% prepared with an ultrafast PbI2 deposition rate, *Sci. Rep.*, 2018, **8**, 442.

44 Q. Jiang, Z. Chu, P. Wang, X. Yang, H. Liu, Y. Wang, Z. Yin, J. Wu, X. Zhang and J. You, Planar-Structure Perovskite Solar Cells with Efficiency beyond 21, *Adv. Mater.*, 2017, **29**, 1703852.

45 Y. Chen, Q. Meng, Y. Xiao, X. Zhang, J. Sun, C. B. Han, H. Gao, Y. Zhang, Y. Lu and H. Yan, Mechanism of PbI$_2$ in situ passivated perovskite films for enhancing the performance of perovskite solar cells, *ACS Appl. Mater. Interfaces*, 2019, **11**, 44101–44108.

46 Q. Meng, Y. Chen, Y. Y. Xiao, J. Sun, X. Zhang, C. B. Han, H. Gao, Y. Zhang and H. Yan, Effect of temperature on the performance of perovskite solar cells, *J. Mater. Sci.: Mater. Electron.*, 2020, **32**, 12784–12792.

47 Z. Xu, Z. Liu, N. Li, G. Tang, G. Zheng, C. Zhu, Y. Chen, L. Wang, Y. Huang, L. Li, N. Zhou, J. Hong, Q. Chen and H. Zhou, A Thermodynamically Favored Crystal Orientation in Mixed Formamidinium/Methylammonium Perovskite for Efficient Solar Cells, *Adv. Mater.*, 2019, **31**, 1900390.

48 M. K. Kim, G.-H. Kim, T. K. Lee, I. W. Choi, H. W. Choi, Y. Jo, Y. J. Yoon, J. W. Kim, J. Lee, D. Huh, S. K. Kwak, J. Y. Kim, D. S. Y. Kim and C. D. Kim, Methylammonium Chloride Induces Intermediate Phase Stabilization for Efficient Perovskite Solar Cells, *Joule*, 2019, **3**, 2179–2192.

49 A. F. Castro-Méndez, J. Hidalgo and J. P. Correa-Baena, The Role of Grain Boundaries in Perovskite Solar Cells, *Adv. Energy Mater.*, 2019, **9**, 149–160.

50 Z. Ni, C. Bao, Y. Liu, Q. Jiang, W. Q. Wu, S. Chen, X. Dai, B. Chen, B. Hartweg, Z. Yu, Z. Holman and J. Huang, Resolving spatial and energetic distributions of trap states in metal halide perovskite solar cells, *Science*, 2020, **367**, 1352–1358.

51 F. Gao, Y. Zhao, X. Zhang and J. You, Recent Progresses on Defect Passivation toward Efficient Perovskite Solar Cells, *Adv. Energy Mater.*, 2019, **10**, 1902650.

52 Q. Wang, B. Chen, Y. Liu, Y. Deng, Y. Bai, Q. Dong and J. Huang, Scaling behavior of moisture-induced grain degradation in polycrystalline hybrid perovskite thin films, *Energy Environ. Sci.*, 2017, **10**, 516–522.

53 N. A. Nadege Ouedraogo, M. Yang, C. He, Y. Chen, X. Zhang, H. Yan, C. B. Han and Y. Zhang, Influence of polytetrafluoroethylene (PTFE) on photovoltaic performance and perovskite solar cell stability, *Sustainable Energy Fuels*, 2020, **4**, 4257–4263.